Evanescent Pressure Gradient Response in the Upper Ocean to Subinertial Wind Stress Forcing of Finite Wavelength

WARREN B. WHITE AND GERARD MCNALLY

Scripps Institution of Oceanography, University of California, San Diego, La Jolla, CA 92093

(Manuscript received 27 May 1986, in final form 29 December 1986)

ABSTRACT

The idea that Ekman transport driven by the mean synoptic wind stress on the f_0-plane is a robust result is true only for infinite scale lengths of the wind stress forcing. For finite scale wavelengths [O(100 km)] and for a range of subinertial frequencies ranging from 2–10 pendulum days, Ekman transport must compete with the transport associated with pressure gradient flow associated with wind-driven evanescent waves that develop in the pycnocline below the mixed layer. This is demonstrated in a schematic model of the upper ocean at midlatitude where the surface mixed layer of depth H lies above a pycnocline of uniform stratification N^2, driven by schematic wind stress that approximates that associated with the passage of storm fronts. It is shown that subinertial response to transient wind forcing at these periods even at infinite wavelength scales favors the anticyclonic response over the cyclonic one; this tendency is maximum at a period of 1 pendulum day, disappearing at 10 pendulum days as the transient subinertial response approaches the exact equilibrium state Ekman response. However, for transient wind stress of finite wavelength, due to the propagation of atmospheric frontal disturbances of wavelength L and period T at speed C_{pz}, the wind-driven response of the mixed layer penetrates downward into the pycnocline. Divergence in mixed layer motions at subinertial frequencies produce evanescent (i.e., vertical attenuating) motion within the upper portion of the pycnocline. The evanescent horizontal motions are directly out of phase with those in the mixed layer; the evanescent vertical motion alters the density field of the pycnocline and, hence, the pressure field over the entire upper ocean. The resulting transient pressure gradient (i.e., geostrophic) response in the mixed layer is directed in the downwind direction, lagging the cross-wind transient Ekman response by 90°. At subinertial periods of 2–10 pendulum days and wavelengths of O(100 km), the magnitude of this transient geostrophic response is on the same order as that of the transient wind-driven Ekman response. Approaching equilibrium state at 10 pendulum days, the ratio of the equilibrium state geostrophic response to the equilibrium state Ekman response in this schematic model is NH/C_{pz}; i.e., the ratio of the internal wave speed scale to the speed scale of propagation of the atmosphere frontal disturbance. Therefore, in the real ocean driven by wind stress of finite wavelength at subinertial frequencies, the transient Ekman response to wind stress forcing represents only part of the total response; a transient geostrophic response also exists that can be as large or larger than the transient Ekman response.

1. Introduction

White (1986) recently discussed the near-inertial response of the upper ocean to wind stress forcing of finite wavelength [i.e., O(100 km)], establishing that the divergence of wind-driven, near-inertial, motions in the mixed layer produced vertical motion at the base of the mixed layer, O(0.1 cm s^{-1}), which acted to pump near-inertial waves in the main pycnocline below, similar to those simulated numerically by Price (1983). These vertical motions altered the density distribution in the main pycnocline and, hence, the pressure field over the entire upper ocean. The ensuing pressure gradient flows were found to be O(1 cm s^{-1}), negligible compared to the near-inertial motions O(10 cm s^{-1}) in the mixed layer. However, further examination of this pressure gradient effect determines that while it is negligible compared to near-inertial motions (i.e., near the 1 pendulum day period), it is not negligible compared to subinertial motion ranging in period from 2–10 pendulum days.

This particular range of subinertial frequencies has been the subject of a number of upper ocean, process-oriented, experiments conducted over the past 10 years (e.g., JASIN, MILE, STREX). In these experiments, the response of the upper ocean current to wind stress forcing has been measured throughout the surface mixed layer and upper portion of the pycnocline below. Yet, these experiments have been conducted under the assumption that the spatial scale of the wind stress forcing was very large. As such, the geostrophic response to wind forcing at subinertial frequencies on spatial scales O(100 km) was not measured routinely as a time series in concert with the upper-ocean current meter observations. Yet, the limited number of pressure gradient measurements that were made in these experiments did indicate their importance in the overall momentum budget at subinertial frequencies (Davis et al., 1981a,b; Weller, 1982; Pollard, 1983). Yet, this pressure gradient effect was considered to have been advected into the experimental region, not locally generated (e.g., Weller, 1982). In the present study, the

possibility is shown that subinertial density and pressure fluctuations can arise locally from the finite wavelength character of the wind stress forcing as a fundamental, and significant, part of the upper ocean transient, wind-driven, response on time scales of 2–10 pendulum days. As such, locally generated pressure gradient fluctuations cannot be neglected in future experiments of this nature.

It is well known from the work of Veronis and Stommel (1956) that the variety of spatial and temporal scales that comprise the wavenumber/frequency domain of atmospheric wind stress forcing excite different classes of free waves in the upper ocean. The higher frequencies excite gravity waves; somewhat lower frequencies excite inertio–gravity waves; and still lower frequencies excite the barotropic and baroclinic Rossby waves. It is in the frequency range between the inertio-gravity waves and the barotropic Rossby waves (called here the "subinertial" frequency range, extending in period from 2–10 pendulum days) that a class of evanescent waves exist that give rise to appreciable fluctuations in the density field of the pycnocline and, hence, in the pressure field of the entire upper ocean. These waves form an important link between the near-inertial waves and the equilibrium state Ekman (1905) response to wind forcing upon the f_0-plane. As such, both the equilibrium state and transient mixed layer response to the wind stress forcing of finite wavelength will be seen to be comprised of a pressure gradient response in addition to an Ekman response. However, while the Ekman response is in the crosswind direction and in phase with the wind stress variability, the pressure gradient response is in the downwind direction and lags it by 90°.

A demonstration of this upper ocean response is made by means of a highly idealized, schematic model, comprised of a surface mixed layer of nominal depth H, overlying a pycnocline of constant stratification N^2 (Fig. 1). This model is driven by an oscillating, meridional-directed, wind stress of zero mean, which is propagated in the positive x direction at a constant speed scale of C_{px}. As such, each subinertial period T is naturally associated with a zonal wavelength L, where

$$L = C_{px} T. \tag{1.1}$$

It is this finite wavelength that gives rise to the penetration of the subinertial mixed layer response into the upper portion of the pycnocline, which in turn leads to a pressure gradient response that affects the vertical profile of wind-driven flow over the entire column. This study differs from earlier ones (e.g., Gill, 1984) where the response in the pycnocline to traveling atmospheric disturbances is expanded in terms of vertical normal modes of superinertial frequency; in fact, this study compliments these earlier studies by conducting the finite wavelength response from the inertio–gravity waves frequency range into the subinertial frequency range on the f_0-plane (i.e., without having to resort to the β-plane approximation). This is done by an examination of the solutions for vertically trapped (evanescent) motions below the mixed layer.

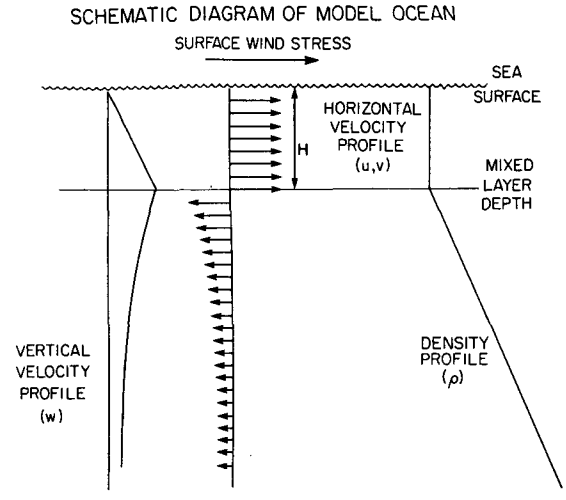

FIG. 1. Schematic diagram of the model ocean, with surface mixed layer driven by surface wind stress, overlying a main pycnocline of constant stratification. Schematic profiles of horizontal and vertical velocity components are representative of wind-driven, subinertial waves.

The results of this theoretical development are qualitatively consistent with the near surface velocity measurements obtained with satellite tracked drifting buoys drogued within the mixed layer during the autumn/winter of 1979 (McNally and White, 1985), where the drogued drifters, independent of windage and waveage, were found to have a large downwind response that lagged the wind stress vector, in addition to the expected Ekman crosswind response that was in phase with the wind stress vector. In this study rotary spectra of both observed and model velocity data are found to be consistent with one another and suggest that the drifting buoys may have been influenced significantly by this downwind geostrophic response. This is in addition to the possibility raised by White (1986) that drifting buoys drogued near the base of the mixed layer should travel in the direction of atmospheric disturbances due to the combination of vertical Reynolds stress divergence and Stokes drift in the upper ocean associated with near-inertial waves of finite wavelength.

2. Free subinertial waves in a uniformly stratified fluid

The basic equations conserve momentum, volume, and mass. Those pertinent to the description of linear subinertial waves (i.e., $\omega < f$) can be written as follows: i.e.,

$$\frac{\partial u'}{\partial t} - fv' + \frac{\partial p'}{\partial x}\frac{1}{\rho_0} = 0$$

$$\frac{\partial v'}{\partial t} + fu' + \frac{\partial p'}{\partial y}\frac{1}{\rho_0} = 0$$

$$g\rho' + \frac{\partial p'}{\partial z} = 0$$

$$\frac{\partial u'}{\partial x} + \frac{\partial v'}{\partial y} + \frac{\partial w'}{\partial z} = 0$$

$$\frac{\partial \rho'}{\partial t} - w' \frac{\rho_0 N^2}{g} = 0 \qquad (2.1a\text{–}e)$$

where u', v', w' follow normal convention in defining the perturbation velocity components, p' is the pressure perturbation, f is the Coriolis parameter [assumed to be a linear function of latitude ($f_0 + \beta y$)], g is the acceleration of gravity, ρ' is the density perturbation, and

$$N^2 = \frac{-g}{\rho_0} \frac{\partial \bar{\rho}}{\partial z}$$

is the Vaisala frequency, taken as constant with depth and horizontal distance.

With five equations in five unknowns (i.e., u', v', w', p', ρ'), manipulation of (2.1) yields

$$\frac{\partial}{\partial t}\left[\left(\frac{\partial}{\partial t}\right)^2 + f_0^2\right] u'_{zz} + N^2 \frac{\partial}{\partial t}[u'_{xx} + u'_{yy}] + \beta N^2 \frac{\partial u'}{\partial x} = 0$$

$$\frac{\partial}{\partial t}\left[\left(\frac{\partial}{\partial t}\right)^2 + f_0^2\right] v'_{zz} + N^2 \frac{\partial}{\partial t}[v'_{xx} + v'_{yy}] + \beta N^2 \frac{\partial v'}{\partial x} = 0$$

$$\frac{\partial}{\partial t}\left[\left(\frac{\partial}{\partial t}\right)^2 + f_0^2\right] w'_{zz} + N^2 \frac{\partial}{\partial t}\left[w'_{xx} + w'_{yy}\right] + \beta N^2 \frac{\partial w'}{\partial x} = 0. \qquad (2.2)$$

These equations yield free, linear, waves of the system; i.e.,

$$\begin{bmatrix} u' \\ v' \\ w' \end{bmatrix} = \begin{bmatrix} u'_0 \\ v'_0 \\ w'_0 \end{bmatrix} e^{i(kx+jy+nz-\omega t)} \qquad (2.3)$$

where k and j are the horizontal wavenumber components, n is the vertical wavenumber component, and ω is the frequency of the waves. Linearity is maintained by requiring that $u'_0 \ll (f_0/k)$, $v'_0 \ll (f_0/j)$, and $w'_0 \ll (f_0/n)$.

The dispersion relation for these waves is given by

$$\omega^3 - \omega\left[f_0^2 + N^2 \frac{(k^2+j^2)}{n^2}\right] - N^2 \frac{\beta k}{n^2} = 0. \qquad (2.4)$$

This expression can be simplified by neglecting terms based upon their time and length scales (Veronis and Stommel, 1956).

For waves of frequency $\omega > f_0$, the dispersion relation in (2.4) reduces to

$$\omega^2 = f_0^2 + N^2\left[\frac{k^2+j^2}{n^2}\right] \qquad (2.5)$$

where the Coriolis parameter is considered a constant with latitude. These waves are called inertio–gravity waves by Veronis and Stommel (1956).

For waves of frequency $\omega \ll f_0$, the dispersion relationship in (2.4) reduces to

$$\omega = \frac{-\beta k}{k^2 + j^2 + (f_0^2 n^2/N^2)} \qquad (2.6)$$

where $N/f_0 n$ is the internal Rossby radius of deformation. This dispersion relation pertains to a set of waves called baroclinic Rossby waves that owe their existence to the meridional derivative (i.e., β) of the Coriolis parameter f. This expression applies for frequencies that are much lower than the inertial frequency (i.e., $\omega^3 \ll N^2\beta k/n^2$), typically on time scales greater than months to years at midlatitude (Veronis and Stommel, 1956).

There does exist another class of waves, called here "subinertial evanescent waves," not discussed by Veronis and Stommel (1956) because of their vertical evanescent character. These waves have significance at frequencies between the inertio–gravity waves and the Rossby waves. Waves at these subinertial frequencies are not free to propagate vertically as are the inertio–gravity and Rossby waves; rather, they are vertically evanescent, trapped to the top of the pycnocline and must be forced from above. They propagate horizontally only by virtue of the propagation of the wind stress disturbance. Yet, like the wind forced Rossby waves they perturb the density field in the pycnocline and, hence, the pressure field over the upper ocean. This leads to a significant relative geostrophic response to wind forcing at these subinertial frequencies. This relative geostrophic response is not confined to the pycnocline; its influence extends upward into the mixed layer and competes with the wind-driven transient Ekman response at subinertial frequencies in the mixed layer.

Therefore, for subinertial waves of imaginary vertical wavenumber and finite horizontal wavelength [O(100 km)], the dispersion relationship in (2.4) reduces to

$$\omega^2 = f_0^2 - \frac{N^2(k^2+j^2)}{n^2} \qquad (2.7)$$

where n^{-1} is *hereafter* defined as the e-folding attenuation scale in the vertical direction. For subinertial waves traveling horizontally on the f_0-plane (i.e., $\beta = 0$) with the wind stress forcing, this vertically evanescent wave is the only one possible; given the frequency (ω) and horizontal wavenumber (k, j) of the subinertial pumping at the top of the main pycnocline, the dispersion relation in (2.7) can be used to determine the e-folding depth scale of penetration (n^{-1}) of the pycnocline response to wind stress curl forcing at these subinertial frequencies. This e-folding depth scale is plotted versus the normalized frequency and horizontal wavenumber from (2.7) in Fig. 2. As can be seen for different subinertial periods ranging from 1–10 pen-

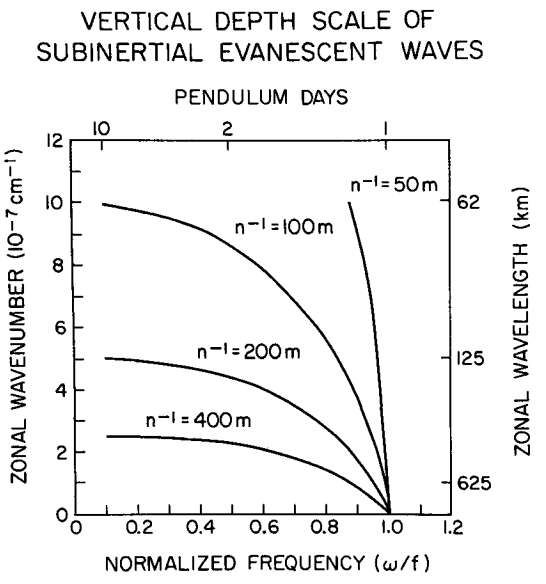

FIG. 2. Vertical e-folding depth scale (n^{-1}) as a function of normalized frequency (ω/f) and wavenumber (k) over the subinertial frequency range (i.e., corresponding in period of 1–10 pendulum days). This is determined from the dispersion relation in (2.7).

dulum days, the zonal wavelength associated with that period [i.e., $L = C_{px}T$ in (1.1)] determines the e-folding depth scale of the evanescent wave. At a particular subinertial frequency, short horizontal wavelengths yield shallow penetration of the evanescent waves, with longer horizontal scales yielding deeper penetration. This relationship between horizontal scale and vertical scale is more prominent at longer periods than periods near the inertial frequency, where large changes in zonal scale length produce small changes in vertical scale length.

3. Wind-driven subinertial waves in the mixed layer

The vertical structure of the schematic model ocean is displayed in Fig. 1. It consists of a surface mixed layer of mean depth H overlying a pycnocline of constant stratification (i.e., N^2 = constant). Because only subinertial waves are concerned here, the model is placed upon an f_0-plane, where $f = f_0$. Wind stress is applied at the sea surface and is set to zero at the base of the mixed layer. No particular profile of stress is assumed within the mixed layer, so that equations governing subinertial horizontal motion in the mixed layer represents those of vertically averaged horizontal motion. Vertical motion at the base of the mixed layer, generated by the divergence of subinertial horizontal motion in the mixed layer, acts as the source of subinertial waves in the pycnocline below.

Linear equations for wind-driven, subinertial, waves in the surface mixed layer are written:

$$\left[\left(\frac{\partial}{\partial t}\right)^2 + f_0^2\right]u' = \frac{\partial \tau^x}{\partial t}\frac{1}{H} + f_0\frac{\tau^y}{H}$$

$$\left[\left(\frac{\partial}{\partial t}\right)^2 + f_0^2\right]v' = \frac{\partial \tau^y}{\partial t}\frac{1}{H} - f_0\frac{\tau^x}{H}$$

$$\left[\left(\frac{\partial}{\partial t}\right)^2 + f_0^2\right]w' = -\mathrm{Div}\frac{\partial \vec{\tau}}{\partial t} - f_0\,\mathrm{curl}_z\vec{\tau}. \qquad (3.1)$$

These equations differ from those displayed in (2.2) with the inclusion of perturbation horizontal kinematic wind stress components (τ^x, τ^y) on the right-hand side, and with the stratification parameter, N^2, and the β parameter set equal to zero.

The kinematic wind stress vector chosen to force the schematic ocean model is defined such that it approximates the zonal passage of frontal disturbances embedded in synoptic storms in the midlatitude North Pacific. Therefore, the wind stress vector is confined to the meridional direction and with the following form:

$$\tau^x = 0$$

$$\tau^y = 2\tau_0 \cos[(k)x - (\omega)t] \qquad (3.2a)$$

where $C_{px} = \omega/k$ represents the speed with which the atmospheric frontal disturbances responsible for the wind stress forcing propagates from west to east as discussed in connection with (1.1). The form chosen of the kinematic wind stress forcing in (3.2a) was done also because it can be easily represented as the sum of a pair of vectors of equal magnitude (τ_0), one of which rotates anticyclonically [$\omega < 0$] and the other of which rotates cyclonically [$\omega > 0$]; i.e.,

$$\tau^x = \tau^x_{+\omega} + \tau^x_{-\omega}$$

$$\tau^y = \tau^y_{+\omega} + \tau^y_{-\omega}, \qquad (3.2b)$$

where

$$\tau^x = \tau_0 \sin[(k)x - (\omega)t]$$

$$\tau^y = \tau_0 \cos[(k)x - (\omega)t] \qquad (3.3)$$

where now ω is allowed to range from $-f_0 < \omega < f_0$ and k is allowed to range from $-k_0 < k < k_0$, where $C_{px} = f_0/k_0 = \omega/k$ is kept constant according to (1.1).

Substitution of (3.3) into (3.1) yields the following particular solution for the mixed layer. The solution is the response to the rotating wind stress vector: i.e.,

$$u'_{\mathrm{Ek}} = \frac{\tau_0}{(f_0+\omega)H}\cos[(k)x - (\omega)t]$$

$$v'_{\mathrm{Ek}} = \frac{-\tau_0}{(f_0+\omega)H}\sin[(k)x - (\omega)t]$$

$$w'_{\mathrm{Ek}|-H} = \frac{\tau_0(k)}{(f_0+\omega)}\sin[(k)x - (\omega)k] \qquad (3.4)$$

where ω ranges from $-f_0 < \omega < f_0$ and k ranges from $-k_0 < k < k_0$. In these solutions, the horizontal velocity

vector has the same sense of rotation as the forcing wind stress vector [given in (3.3)], but is directed 90° to the right of the wind stress vector. However, as can be observed, the amplitudes of the response are quite different for cyclonic ($0 < \omega < f_0$) and anticyclonic ($-f_0 < \omega < 0$) wind stress forcing. The relative amplitude of the horizontal velocity vector as a function of frequency over the subinertial frequency range (i.e., with frequencies ranging from $-f_0$ to $+f_0$) is shown in upper panel of Fig. 3. The solution to cyclonically rotating wind stress vector ($0 < \omega < f_0$) has finite response at the frequency f_0 (i.e., $\tau_0/2f_0H$) and tends toward the steady state Ekman response (i.e., τ_0/Hf_0) at lower frequency (i.e., as $\omega \rightarrow 0.1f_0$). On the other hand, the solution to anticyclonically rotating wind stress vector ($-f_0 < \omega < 0$) has infinite response at the frequency $-f_0$ [i.e., the inertial resonant response (White, 1986)] and also tends toward the equilibrium state Ekman response as $\omega \rightarrow -0.1f_0$. At the frequency ($\pm 0.1f_0$), corresponding to a period of ten pendulum days, the two solutions are essentially in equilibrium state Ekman balance (i.e., τ_0/f_0H). However, for the subinertial frequency range, corresponding to periods ranging between 2 and 10 pendulum days, the anticyclonically rotating solution dominates the cyclonically rotating one. This is true regardless of the horizontal scale $2\pi k^{-1}$.

Therefore, the wind stress forcing of synoptic period storms (i.e., 2–10 pendulum days) yields a response in the mixed layer that favors the anticyclonic rotation

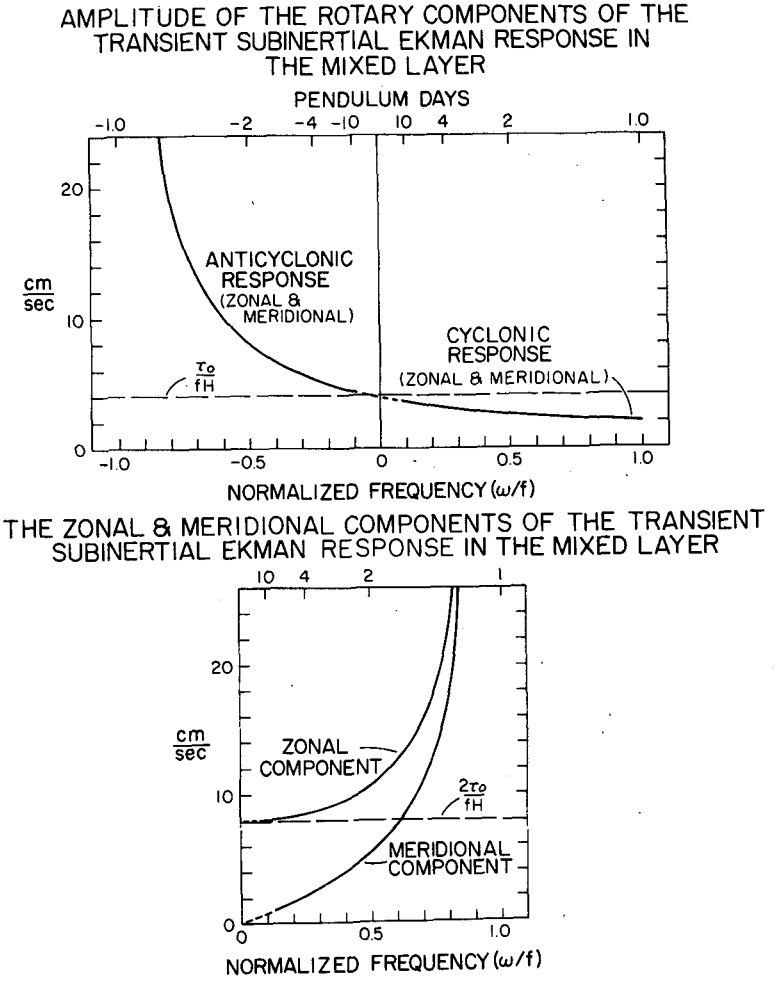

FIG. 3. (Upper panel) Amplitude of the direct, wind-driven, horizontal current response in the mixed layer to both an anticyclonically rotating wind stress vector (negative frequencies) and a cyclonically rotating wind stress vector (positive frequencies) as a function of normalized frequency. The horizontal asymptote is the equilibrium Ekman response (i.e., τ_0/f_0H). (Lower panel) Amplitude of the sum of the anticyclonically and cyclonically rotating velocity vectors displayed in the upper panel as a function of normalized frequency. This is the amplitude of the direct mixed layer transient (Ekman) response to the wind stress forcing given in (3.2). The horizontal asymptote is the equilibrium state crosswind Ekman response (i.e., $2\tau_0/f_0H$).

over the cyclonic rotation. This kind of asymmetry in the amplitude of the mixed layer response to wind stress forcing rotating cyclonically and anticyclonically has been observed in the mixed layer during both MILE (Davis et al., 1981a,b) and JASIN (Weller, 1982; Weller and Halpern, 1983). This was amply demonstrated as well in the hurricane numerical model study of Price (1983).

The rotary spectra of the near surface velocities of satellite tracked drifting buoys used in a study of mixed layer response to autumn/winter surface wind stress forcing of 1979 (McNally and White, 1985) are displayed in the left panel of Fig. 4. These spectra were formed from the ensemble average of spectral estimates from 18 sixteen day records of velocity taken from three drifters drogued at 60 m (i.e., in the mixed layer) during this autumn/winter period. In this figure, the spectral energy density of that portion of drifting buoy motion rotating anticyclonically (solid curve) had much larger magnitude than the remaining portion rotating cyclonically (dashed curve), although the difference is only barely statistically significant. The observed ratio of the spectral energy density of these rotary components is plotted in the right panel, together with that derived theoretically from (3.4) (see Fig. 3). These ratios can be seen to be parallel to one another. The observed ratio is generally greater than that derived theoretically, although not at the statistically significant level. The difference between the model and observed ratios will be made clear in a subsequent section when the transient geostrophic response is added to the transient, direct, wind-driven (Ekman), mixed layer response.

Having expressed the total wind stress vector (3.2) in terms of its cyclonic and anticyclonic parts in (3.3), it was possible to determine the cyclonic and anticyclonic solutions in (3.4), where $-f_0 < \omega < f_0$. Now, the transient Ekman solution to the wind stress forcing in (3.2) can be written:

$$U'_{\mathrm{Ek}} = \frac{\tau_0}{(f_0-\omega)_H}\left[\frac{2f_0}{(f_0+\omega)}\right]\cos[(k)x-(\omega)t]$$

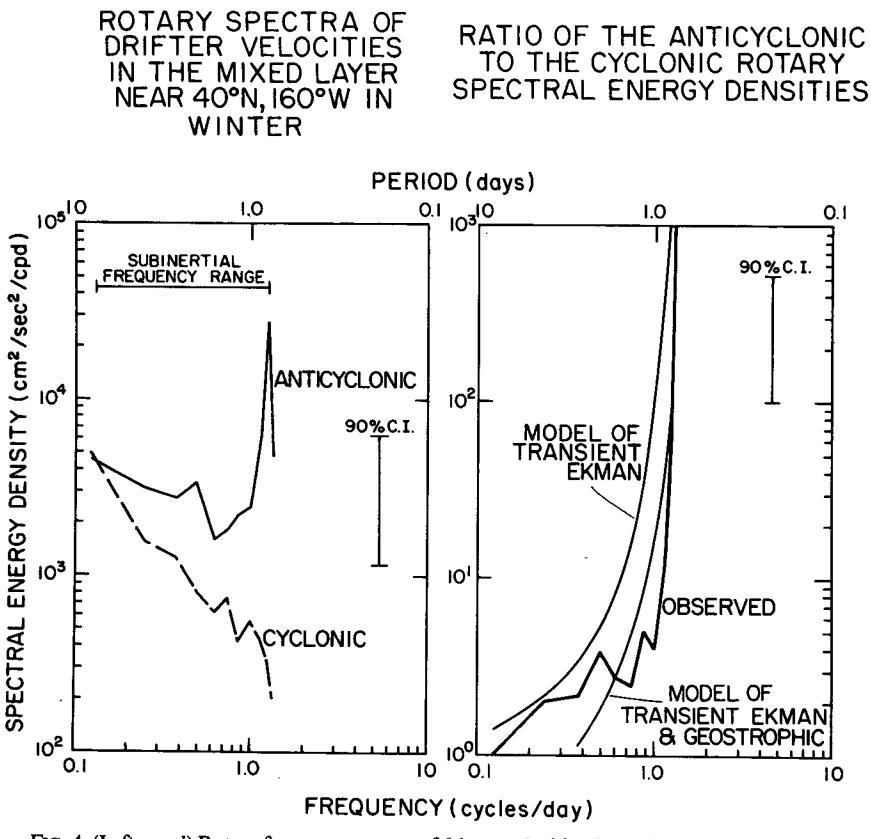

FIG. 4. (Left panel) Rotary frequency spectra of 6-hour velocities determined from the trajectories of satellite-tracked drifting buoys drogued at 60 m near 40°N, 160°W during the fall/winter of 1979 (McNally and White, 1985). These rotary spectra are for the anticyclonic and cyclonic portions of the time varying velocity vectors. See text for further details. (Right panel) The ratio of the spectral energy density of anticyclonic to cyclonic rotary spectra as a function of frequency, together with that predicted by the model solutions in (3.4) (i.e., transient Ekman model for the mixed layer) and later that predicted by the model solutions in (4.1) leading to (6.1) (i.e., transient Ekman plus transient geostrophic response for the mixed layer).

$$V'_{Ek} = \frac{\tau_0}{(f_0-\omega)H}\left[\frac{2\omega}{(f_0+\omega)}\right]\sin[(k)x-(\omega)t]$$

$$W'_{Ek|_{-H}} = \frac{-\tau_0}{(f_0-\omega)}\left[\frac{2f_0}{(f_0+\omega)}\right](k)\sin[(k)x-(\omega)t] \quad (3.5)$$

where now $0 < \omega < f_0$. This solution was obtained by summing the cyclonic and anticyclonic portions of the solutions given in (3.4), keeping in mind that ranging ω in (3.4) from $-f_0$ to f_0 also means ranging k from $-k_0$ to k_0, since $\omega/k = C_{px}$, which is assumed constant in this model development. Comparing the response in (3.5) to the wind stress forcing in (3.2) finds the zonal velocity component (i.e., crosswind component) tending to the equilibrium state Ekman response (i.e., $U'_{Ek} = 2\tau_0/Hf_0$) as $\omega \to 0.1 f_0$, with the meridional velocity component (i.e., downwind component) tending to zero, as $\omega \to 0.1\, f_0$ (displayed in the lower panel of Fig. 3). The meridional downwind component of the response increases in magnitude with increasing frequency throughout the subinertial frequency range, so that at the near-inertial frequency (i.e., $\omega \to f_0$) it has the same magnitude as the zonal crosswind component (see also White, 1986), approaching very large values.

The magnitude of the response in the subinertial frequency range (Fig. 3) and in subsequent figures depends upon the magnitude of the parameters τ_0, H, f_0, N and $C_{px}(\omega/k)$. For these parameters, scale magnitudes for τ_0, H, f_0, N and C_{px} are chosen (Table 1) as representative of those observed during the MILE Experiment (Davis et al., 1981a,b) in the eastern midlatitude North Pacific. This particular field experiment was chosen as an example because it was designed to detect subinertial transient Ekman flow in the mixed layer and both superinertial and subinertial motion in the upper portion of the pycnocline below. The horizontal speed of subinertial waves was not measured at MILE, but is estimated from the mean wind scale (i.e., approximately 1 m s^{-1}) that can be considered to have advected atmospheric frontal disturbances past the MILE experimental location. This yields a zonal scale magnitude for the inertial wave (i.e., $2\pi k_0^{-1} = C_{px}2\pi f_0^{-1}$) also given in Table 1. It remains to be established whether the mean wind scale also represents the horizontal translation vector of atmospheric frontal disturbances in this region. Regardless, the scale magnitudes in Table 1 lead to scale magnitudes for both near-inertial motions, subinertial motions, and equilibrium state Ekman solutions that are consistent with those measured during MILE (see White, 1986, as well). Moreover, the choice of scales in Table 1 maintains the linearity of the solutions [e.g., $|U'_{Ek}| \ll (\omega/k)$].

TABLE 1. Scale magnitude of model parameters approximating conditions at the mixed layer experiment (MILE 1) located at 49°N, 145°W during August–September 1977.

$\tau_0 = 2$ dyn cm^{-2}
$H = 5\times10^3$ cm
$C_{px} = 100$ cm s^{-1}
$2\pi f_0^{-1} = 6\times10^4$ sec (17 h)
$2\pi k_0^{-1} = 6\times10^6$ cm (60 km)
$2\pi N^{-1} = 6\times10^2$ sec (0.17 h)

4. Pumped subinertial waves in the pycnocline

Subinertial waves of finite wavelength ($2\pi k^{-1}$) in the pycnocline of the schematic model ocean, displayed in Fig. 1, are driven by the vertical velocity perturbation at the base of the surface mixed layer, induced by "subinertial pumping" in the mixed layer (i.e., $w'_{Ek|_{-H}}$). The magnitude of the vertical motion is dependent not only on the frequency of the response, but also on its wavenumber (k), where from (1.1), $C_{px} = \omega/k$. The vertical motion of free evanescent waves in the pycnocline, given in (2.3) (where the vertical wavenumber component n is considered imaginary), must match the forced vertical motion $w'_{Ek|_{-H}}$ given in (3.4). The horizontal motion of free evanescent waves in the pycnocline are then required to be internally consistent with the set of equations (2.1) and (2.2), as described in connection with the derivation of the dispersion relation in (2.7) and its related assumptions.

The solution in the stratified region of the pycnocline below the mixed layer can be written for subinertial pumping stemming from the rotating velocity vector in (3.4):

$$u'_{pc} = \frac{-\tau_0 n}{(f_0+\omega)}\cos[(k)x-(\omega)t]e^{n(z+H)}$$

$$v'_{pc} = \frac{-\tau_0 n}{(f_0+\omega)}\frac{(\omega)}{f_0}\sin[(k)x-(\omega)t]e^{n(z+H)}\left(1+\frac{N^2}{C_{px}{}^2n^2}\right)$$

$$w'_{pc} = \frac{-\tau_0 k}{(f_0+\omega)}\sin[(k)x-(\omega)t]e^{n(z+H)} \quad (4.1)$$

where as in (3.4) ω ranges from $-f_0 < \omega < f_0$ and k ranges from $-k_0 < k < k_0$, representing solutions for both cyclonic ($0 < \omega < f_0$) and anticyclonic ($-f_0 < \omega < 0$) motions, and n is of positive value always. The vertical velocity component in (4.1), evaluated at $z = -H$, equals that given at the base of the mixed layer in (3.4). The zonal velocity component (u'_{pc}) in (4.1) is computed directly from w'_{pc} through the continuity equation [2.1(d)], where $\partial v'/\partial y = 0$. The meridional velocity component (v'_{pc}) in (4.1) is computed from the zonal momentum equation [2.1(a)] from knowledge of u'_{pc} and p'_{pc}. In (4.1b), the zonal pressure gradient portion ($N^2/C_{px}{}^2n^2$) can be on the same order of magnitude as the local zonal acceleration portion (1 in brackets). At near-inertial frequencies (i.e., $\omega \to -f_0$) the pressure gradient forces in (2.1a) and (2.1b) are negligible compared to the inertial forces (White, 1986), but at subinertial frequencies they can be significant

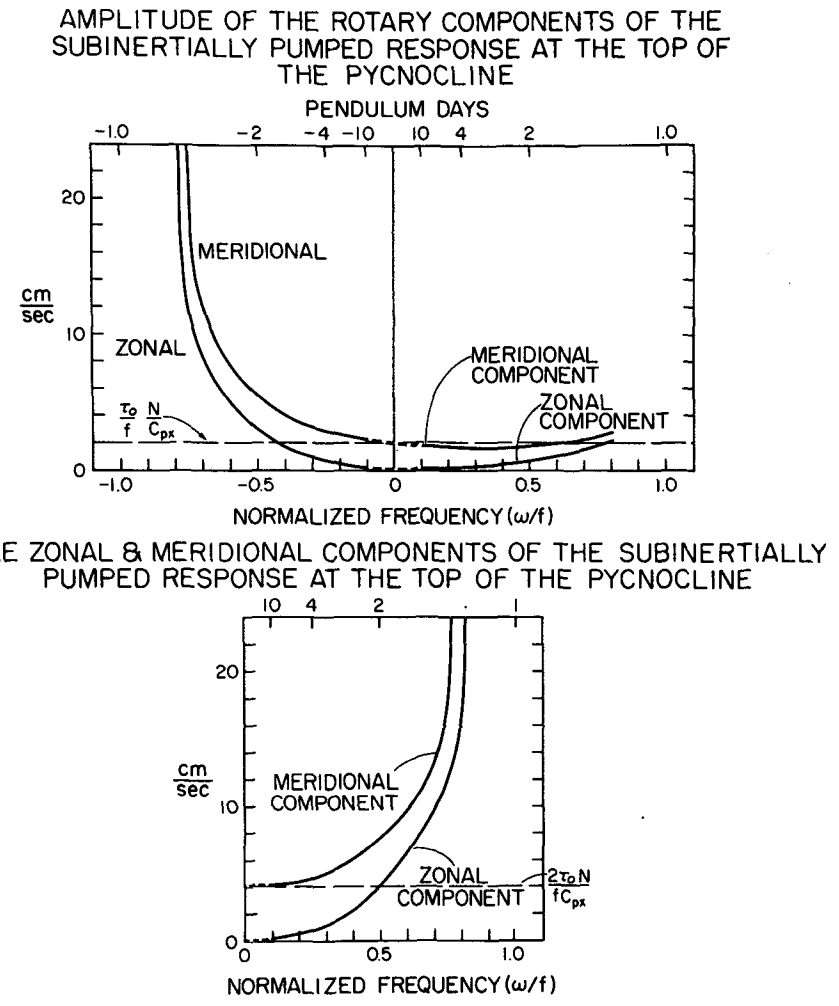

FIG. 5. (Upper panel) Amplitude of the horizontal velocity response at the top of the pycnocline to both anticyclonic (negative frequencies) and cyclonic (positive frequencies) subinertial pumping at the base of the mixed layer. The horizontal asymptote is the equilibrium state geostrophic response. (Lower panel) Amplitude of the total horizontal velocity response at the top of the pycnocline to the total wind stress forcing given in (3.2). The horizontal asymptote is the equilibrium state geostrophic downwind response (i.e., $2\tau_0 N/f_0 C_{px}$).

(i.e., depending upon the size of k). Knowledge of p'_{pc} in (2.1a) is gained from w'_{pc} through (2.1e) and (2.1c). Use of the dispersion relation (2.7) in (4.1b) leads u'_{pc} and v'_{pc} to satisfy (2.1b).

Similar to the transient Ekman response in the mixed layer, the pumped pycnocline response has the anticyclonic amplitude larger than the cyclonic amplitude (see the upper panel of Fig. 5). However, unlike the mixed layer transient Ekman response in (3.4), the amplitudes of the meridional and zonal components in the main pycnocline (4.1) are *unequal*.

The solution in the main pycnocline to the wind stress forcing in (3.2) can be written as it was in (3.5):

$$U'_{pc} = \frac{-\tau_0 n}{f_0 - \omega}\left[\frac{2f_0}{(f_0+\omega)}\right]\cos[(k)x-(\omega)t]e^{n(z+H)}$$

$$V'_{pc} = \frac{-\tau_0 n}{f_0 - \omega}\left[\frac{2\omega}{(f_0+\omega)}\right]\sin[(k)x-(\omega)t] \times e^{n(z+H)}\left(1+\frac{N^2}{C_{px}{}^2 n^2}\right)$$

$$W'_{pc} = \frac{-\tau_0}{f_0 - \omega}\left[\frac{2f_0}{(f_0+\omega)}\right](k)\sin[(k)x-(\omega)t]e^{n(z+H)} \quad (4.2)$$

where now $0 < \omega < f_0$ and $0 < k < k_0$. Again, this solution was obtained by summing the cyclonic and anticyclonic portions of the solutions given in (4.1), again keeping in mind that ranging ω in (4.1) from $-f_0$ to f_0 also means ranging k from $-k_0$ to k_0, since $C_{px} = \omega/k$ which is assumed constant in this model development. Both the zonal and meridional components

of the pycnocline response (4.2) are seen to be of the opposite sign to that of the mixed layer response (3.5) (see schematic diagram in Fig. 1).

The variation of the amplitudes of the zonal and meridional components of the total pycnocline response (4.2) as a function of frequency in the subinertial frequency range is shown in the lower panel of Fig. 5. At the low frequency end of the subinertial range of frequencies (i.e., $\omega \to 0.1f_0$) the amplitude of the meridional component (i.e., downwind component) approaches a value of $2\tau_0 N/f_0 C_{px}$ (this result is explained in the next section), whereas in the mixed layer (see the lower panel of Fig. 3) the amplitude of the meridional component of the Ekman response tends toward zero. On the other hand, the amplitude of the zonal component (i.e., crosswind component) of the pycnocline response (4.2) tends toward zero (as $\omega \to 0.1f_0$ and $n \to 0$), whereas that in the mixed layer response approaches $2\tau_0/f_0 H$ (i.e., the equilibrium state Ekman response). At the high frequency end (i.e. near-inertial frequencies) the zonal and meridional components in the pycnocline approach relatively large values, as do their counterparts in the mixed layer.

The result that rotary components of the wind-driven flow below the mixed layer are directed oppositely to wind-driven (transient Ekman) flow in the mixed layer has been observed repeatedly. In the JASIN experiment, Weller (1982) and Weller and Halpern (1983) found subinertial wind-driven flow below the mixed layer directed approximately 180° to that in the mixed layer (e.g., see Fig. 11 in Weller and Halpern, 1983). This occurred over a record length extending from 1 August to 5 September in the North Atlantic (Weller and Halpern, 1983), at a time when for at least half this period the decorrelation spatial scale of the subinertial motion was less than 44 km. This same observation of oppositely directed subinertial motion above and below the mixed layer depth was also observed during the MILE experiment (Davis et al., 1981a,b). This has been diagrammed schematically in Fig. 1.

5. Geostrophic adjustment in the main pycnocline

The meridional velocity component (i.e., downwind component) in the pycnocline (4.2) consists of two parts (i.e., $V'_{pc} = V'_g + V'_a$). The first of these, V'_g, results from the zonal pressure gradient in (2.1a), which leads to transient relative geostrophic flow throughout the pycnocline, where

$$V'_g = \frac{-2\tau_0 n\omega}{(f_0-\omega)(f_0+\omega)} \frac{N^2}{C_{px}{}^2 n^2} \sin[(k)x-(\omega)t]e^{n(z+H)}. \tag{5.1}$$

The second part, V'_a, results from the local acceleration of zonal velocity in (2.1a) where

$$V'_a = \frac{-2\tau_0 n\omega}{(f_0-\omega)(f_0+\omega)} \sin[(k)x-(\omega)t]e^{n(z+H)}. \tag{5.2}$$

The ratio of the amplitude of V'_g/V'_a is $N^2/(C_{px}{}^2 n^2) = (f_0-\omega)(f_0+\omega)/\omega^2$, where n is determined from the dispersion relation (2.7) and $C_{px} = \omega/k$. This ratio tends toward zero at the higher frequency, or near-inertial, end of the subinertial frequency range, indicating that V'_g is negligible at those frequencies (see also White, 1986). The relative amplitude of V'_g (i.e., with respect to V'_a) increases as the frequency decreases toward the low frequency end of the subinertial frequency range, so that $V'_g = V'_a$ at a period of ~1.4 pendulum days. The total meridional downwind component, $V'_{pc} = V'_g + V'_g$, in the pycnocline tends to a finite, equilibrium state, value at low frequency (see lower panel of Fig. 5). This steady state value is the geostrophic component of the flow, $V'_{pc} = V'_g$, as V'_a tends to zero as $\omega \to 0.1f_0$. For the same reason, $U'_{pc} = U'_a$ tends to zero as $\omega \to 0.1f_0$. Therefore, the amplitude of V'_g in (5.1) asymptotically approaches $(2\tau_0/f_0)(N/C_{px})$ as $\omega \to 0.1f_0$ [i.e., where from (2.7) $kN/f_0 n \to 1$].

6. Total subinertial response in the mixed layer

The meridional component (i.e., downwind component) in the upper ocean's mixed layer response to subinertial wind stress forcing of finite wavelength is also comprised of two parts. The first part is the transient direct wind-driven (Ekman) response (V'_{Ek}) in the mixed layer, discussed in section 3 and given in (3.5). The second part is the transient geostrophic response (V'_g), resulting from the pressure fluctuations in the main pycnocline due to the penetration of the wind-driven response into the main pycnocline via the vertically evanescent subinertial waves, discussed in the previous section and given in (5.1). This second part does not alter the divergence of wind-driven flow in the mixed layer since the geostrophic flow is nondivergent on the f_0-plane. Therefore, in the present schematic situation, the wind-driven subinertial transient Ekman response in the mixed layer, given in (3.5), is modified by the downwind component, V'_g, from (5.1) evaluated at $z = -H$. Since horizontal and vertical density gradients are considered in this schematic model not to exist in the mixed layer, the relative geostrophic flow in the mixed layer has no vertical shear and is therefore uniform from the base of the mixed layer upward to the sea surface. Therefore, the *total* meridional velocity component (i.e., downwind component) in the mixed layer becomes ($V'_{MT} = V'_{Ek} + V'_g$):

$$V'_{MT} = \frac{2\tau_0}{(f_0-\omega)H}\left[\frac{\omega}{(f_0+\omega)} - \frac{HN}{C_{px}}\frac{(f_0-\omega)^{1/2}}{(f_0+\omega)^{1/2}}\right] \times \sin[(k)x-(\omega)t] \tag{6.1}$$

where ω ranges from $0 < \omega < f_0$ and k ranges from $0 < k < k_0$. The first term in brackets represents the transient direct wind-driven (Ekman) response from (3.5) and the second term in brackets represents the transient relative geostrophic flow from (5.1). The total

is displayed in Fig. 6. Clearly, as $\omega \to f_0$, the effect of the pressure gradient becomes negligible compared to the direct near-inertial response. But as $\omega \to 0.1f_0$, (i.e., as ω ranges through the subinertial frequencies toward $0.1f_0$) the meridional downwind component of the transient direct wind-driven (Ekman) response in the mixed layer diminishes to zero (see the lower panel of Fig. 3), while the meridional transient relative geostrophic flow remains nonzero. In fact, the total meridional downwind response in the mixed layer tends toward

$$V'_{MT} = \frac{-2\tau_0}{f_0}\frac{N}{C_{px}}\sin[(k)x-(\omega)t] \quad \text{as} \quad \omega \to 0.1f_0, \tag{6.2}$$

which is equal to the geostrophic portion of flow (i.e., $V'_{MT} \to V'_g$ as $\omega \to 0.1f_0$). For subinertial periods (i.e., 2–10 pendulum days) the total meridional velocity component in the mixed layer lags the meridional component of wind stress given in (3.2) by 90° (i.e., a quarter period).

Plotting the total zonal (i.e., crosswind) and meridional (i.e., downwind) velocity amplitudes for the mixed layer on the same graph (Fig. 6) shows the mixed layer amplitude response to the transient meridional wind stress [see (3.2)]. Compare this with the lower panel of Fig. 3. For subinertial periods, as the amplitude of the zonal component (i.e., crosswind component)

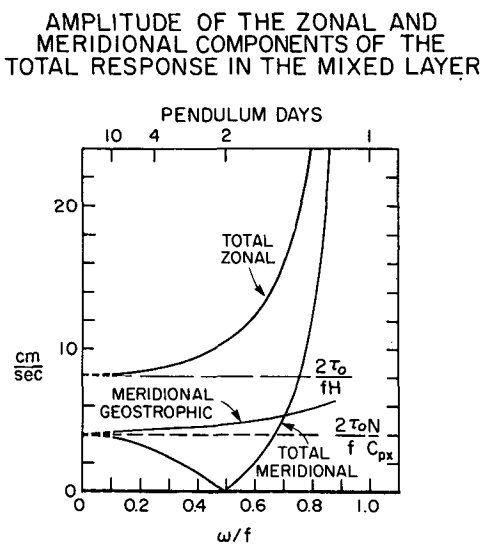

FIG. 6. Amplitude of the wind-driven zonal transient Ekman (crosswind) response in the mixed layer (repeated from Fig. 3b), together with the meridional geostrophic (downwind) response, both in response to the wind stress forcing given in (3.2). Also displayed is the amplitude of the sum of the meridional transient Ekman response and the meridional transient geostrophic response in the mixed layer. The horizontal asymptotes for both the equilibrium state Ekman crosswind response (i.e., $2\tau_0/f_0H$) and the equilibrium state geostrophic downwind response (i.e., $2\tau_0N/f_0C_{px}$) are displayed.

of the response, given in (3.5) and unaffected by the geostrophic response, approaches the equilibrium state Ekman response (i.e., $2\tau_0/f_0H$), the amplitude of the meridional component (i.e., downwind component), given in (6.1) and including the transient geostrophic response, approaches the equilibrium state geostrophic response i.e., $(2\tau_0/f_0)N/C_{px}$. In the absence of this geostrophic portion of the total meridional velocity component within the mixed layer, this component would tend to zero as Ekman theory would predict in response to the wind stress given in (3.2). This is further diagrammed with the aid of the time sequence of hodographs in Fig. 7, showing the schematic equilibrium response (i.e., where $\omega \to 0.1f_0$) to a complete cycle of the meridional wind stress variability given in (3.2).

The ratio of the amplitudes of the equilibrium state downwind geostrophic response to the equilibrium state crosswind Ekman response in the mixed layer of this schematic model is NH/C_{px}; i.e., the ratio of the internal wave speed scale to the zonal speed scale of the atmospheric frontal disturbance. If this ratio becomes greater than unity, then at a point a relatively weak equilibrium state Ekman response will result in phase with the wind stress vector but directed 90° to the right of it and a relatively strong geostrophic response will ensue, lagging the wind stress vector by 90° in time but directed downwind. This is qualitatively consistent with the observations of satellite-tracked drogued drifters in the autumn/winter of 1979 (McNally and White, 1985); i.e., under subinertial storm forcing the drogued drifters observed an equilibrium state crosswind Ekman response in the mixed layer that was in phase with the wind stress *and* an equilibrium downwind response in the mixed layer, lagging the wind stress by 6–12 hours. This lag in time is less than this schematic model would predict and suggests other mechanisms may be operating as well to drive the drogued drifters in the downwind direction (see White, 1986). However, evidence that the geostrophic response does exist in the satellite-tracked drifting buoy data can be seen by plotting the ratio of the anticyclonic response to the cyclonic response in the mixed layer both *without* the geostrophic response and *with* the geostrophic response (Fig. 4). As already discussed in section 3, the ratios of both the observed drifter response and the theoretical mixed-layer response (with geostrophic response excluded) parallel one another over the subinertial frequency range, but the theoretical ratio is greater everywhere. This is accounted for by including the geostrophic response given in (4.1); i.e., its ratio agrees better with that observed (see Fig. 4, left panel).

7. Discussion and conclusion

The results of this study are pertinent to the interpretation of measurements made during a number of

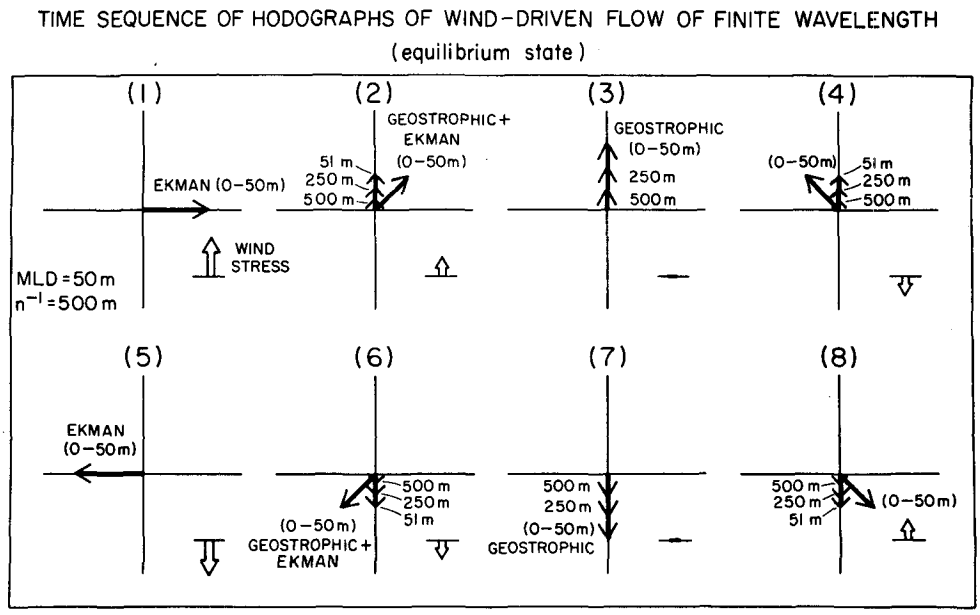

FIG. 7. Time sequence (1–8) of hodographs of the equilibrium state of the wind-driven flow in the mixed layer and upper pycnocline. The finite wavelength of the wind stress forcing was chosen such that the equilibrium state geostrophic flow in the mixed layer has a magnitude equal to the equilibrium state Ekman flow (i.e., $NH/C_{px} = 1$).

process oriented field experiments designed to observe the mixed layer response to wind stress at subinertial frequencies (i.e., 2–10 pendulum days). In the interpretation of both the MILE experiment (Davis et al., 1981a,b) and the JASIN experiment (Weller, 1982; Weller and Halpern, 1983; Pollard, 1982) the observation that rotary subinertial motions in the mixed layer did not conform consistently to transient Ekman theory, and that pycnocline motion existed that was correlated with the wind stress forcing, but oppositely directed to that observed in the mixed layer, was unexpected. Yet, in the present study, both of these observations are, qualitatively at least, consistent with the principles expressed within this schematic model.

The presence of horizontal scales of O(100 km) in the wind stress forcing at subinertial frequencies (i.e., corresponding to periods of 2–10 pendulum days) leads in the model to the penetration of the direct wind-driven current into the pycnocline, with a depth scale given by the horizontal length scale of the wind stress (see Fig. 2). This penetration of the wind-driven response into the main pycnocline is achieved by subinertial pumping (i.e., divergence in the mixed layer transport induced by wind stress curl) at the base of the surface mixed layer. This subinertial pumping excites evanescent waves in the pycnocline which deforms the density field, altering the pressure field over the entire column. The transient geostrophic flow at these subinertial frequencies that results from these pressure gradient responses can be as large, or larger, than the direct, wind-driven, transient Ekman response in the mixed layer. Its relative strength (i.e., ratio of the equilibrium state downwind geostrophic response to the equilibrium state crosswind Ekman response at periods of 5–10 days) is the ratio (i.e., NH/C_{px}) of the internal wave speed (NH) scale to the speed (C_{px}) scale of the wind stress frontal disturbances.

Therefore, according to this model, wind stress frontal disturbances that propagate at speeds similar to those of internal waves (i.e., NH) achieve significant penetration of the wind-driven response into the main pycnocline at subinertial frequencies, resulting in an equilibrium downwind pressure gradient response in the mixed layer that is on the same order of magnitude as the equilibrium crosswind Ekman response at subinertial frequencies.

In both the MILE experiment and the JASIN experiment, rotary components of flow existed below the mixed layer directed opposite to Ekman flow in the mixed layer at subinertial frequencies, coherent with the wind stress. This alone is evidence for the existence of horizontal length scales of the wind stress forcing affecting the experimental situation, with near-inertial and subinertial pumping acting to generate wind-driven Ekman motions below the mixed layer of opposite sign to that in the mixed layer. According to the present study, this also indicates the presence of a significant transient downwind pressure gradient (i.e., geostrophic) flow throughout the upper portion of the pycnocline and in the mixed layer. In the mixed layer, this transient geostrophic downwind flow is superimposed upon the transient crosswind Ekman response and may explain

the inability of these field experiments to relate mixed layer motion directly to the local wind stress via equilibrium state (or transient) Ekman theory. Evidence (see Fig. 4) also indicates that the transient downwind geostrophic response may have had a significant influence upon the trajectories of satellite-tracked drifting buoys deployed at midlatitude in the autumn/winter mixed layer (McNally and White, 1985).

Another result of this model is the recognition that the sign of rotation of the wind stress vector affects the magnitude of the direct wind-driven response, independent of horizontal length scale consideration. Pollard (1970) and Pollard and Millard (1970) established the importance of vector rotation in the excitement of near-inertial waves, but this point has not been carried into the subinertial frequency range (i.e., 2–10 pendulum days). Wind stress vectors rotating in the anticyclonic direction produce magnitudes significantly above the equilibrium state Ekman response for periods of 1–5 pendulum days, whereas wind stress vectors rotating cyclonically produce magnitudes significantly below (see the upper panel of Fig. 3). This indicates that the oceanic response, at subinertial frequencies, to a cyclonic storm, similar to that modeled by Price (1983), will yield a larger response on the right side of the storm path (i.e., where the wind stress vector rotates anticyclonically) than on the left (i.e., where this wind stress vector rotates cyclonically), even though Price's (1983) model storm was scaled to represent a hurricane. Price (1983) does observe this in the near-inertial response, and it would logically extend to the subinertial responses. Price (1983) also observed a significant pressure gradient response on the near-inertial time scale that is compatible with the present results. This result is length scale dependent. It remains to be seen whether these same kinds of space scales are embedded in the much larger synoptic storms at midlatitude in the guise of frontal disturbances and shear lines. If so, as has been assumed in this study, then consideration of such scales will have to be taken into consideration of future field experiments designed to detect wind-driven subinertial motion in the upper ocean.

Acknowledgments. Appreciation is extended to Robert Haney, who as co-editor of the Journal of Physical Oceanography made helpful suggestions leading to improvement in the quality and readability of this manuscript. This work was conducted with the support of the Ocean Research Division at Scripps Institution of Oceanography at the University of California, San Diego in La Jolla, California.

REFERENCES

Davis, R., R. deSzoeke, D. Halpern and P. Niiler, 1981a: Variability in the upper ocean during MILE. Part I: The heat and momentum balances. *Deep-Sea Res.*, **28A,** 1427–1451.

——, —— and P. Niiler, 1981b: Variability in the upper ocean during MILE. Part II: Modeling the mixed layer response. *Deep-Sea Res.*, **28A,** 1453–1475.

Ekman, V., 1905: On the influence of the earth's rotation on ocean currents. *Ark. Mat. Astron. Fys.*, **2,** 1–52.

Gill, A. E., 1984: On the behavior of internal waves in the wakes of storms. *J. Phys. Oceanogr.*, **14,** 1129–1151.

McNally, G., and W. B. White, 1985: Wind driven flow in the mixed layer observed by drifting buoys during autumn/winter in the midlatitude North Pacific. *J. Phys. Oceanogr.*, **15,** 684–694.

Pollard, R. T., 1970: On the generation by winds of inertial waves in the ocean. *Deep Sea Res.*, **17,** 795–812.

——, 1982: Observations of the structure of the upper ocean: Wind driven momentum balance. *Phil. Trans. Roy. Soc. London,* **A380,** 407–425.

——, and R. C. Millard, 1970: Comparison between observed and simulated wind-generated inertial oscillations. *Deep Sea Res.*, **17,** 813–821.

Price, J., 1983: Internal wave wake of a moving storm. Part I: Scales, energy budget and observations. *J. Phys. Oceanogr.*, **13,** 949–965.

Veronis, G., and H. Stommel, 1956: The action of a variable wind stress on a stratified ocean. *J. Mar. Res.*, **15,** 43–75.

Weller, R. A., 1982: The relation of near-inertial motion observed in the mixed layer during the JASIN (1978) experiment to the local wind stress and to the quasi-geostrophic flow field. *J. Phys. Oceanogr.*, **12,** 1122–1136.

——, and D. Halpern, 1983: The velocity structure of the upper ocean in the presence of surface forcing and mesoscale eddies. *Phil. Trans. Roy. Soc. London,* **A380,** 327–340.

White, W. B., 1986: Vertical Reynolds stress divergence in the upper ocean associated with linear wind-driven near-inertial waves of finite wavelength. *J. Phys. Oceanogr.*, **16,** 1190–1203.